

ECCENTRIC BLACK HOLE-NEUTRON STAR MERGERS

BRANSON C. STEPHENS

Center for Gravitation and Cosmology, University of Wisconsin-Milwaukee, Milwaukee, WI 53211, USA.

WILLIAM E. EAST AND FRANS PRETORIUS

Department of Physics, Princeton University, Princeton, NJ 08544, USA.

Draft version November 7, 2018

ABSTRACT

Within the next few years gravitational waves (GWs) from merging black holes (BHs) and neutron stars (NSs) may be directly detected, making a thorough theoretical understanding of these systems a high priority. As an additional motivation, these systems may represent a subset of short-duration gamma-ray burst (sGRB) progenitors. BH-NS mergers are expected to result from primordial, quasi-circular inspiral as well as dynamically formed capture binaries. The latter channel allows mergers with high eccentricity, resulting in a richer variety of outcomes. We perform general relativistic simulations of BH-NS interactions with a range of impact parameters, and find significant variation in the properties of these events that have potentially observable consequences, namely the GW signature, remnant accretion disk mass, and amount of unbound material.

Subject headings: gravitation—gravitational waves—black hole physics—stars: neutron—Gamma-ray burst: general

1. INTRODUCTION

Merging binaries consisting of black holes (BHs) and neutron stars (NSs) are prime targets for observation by ground-based gravitational wave (GW) detectors (such as LIGO, Abramovici et al. 1992) and may be the progenitors of some short-hard gamma-ray bursts (sGRBs, Narayan et al. 1992). The great diversity of sGRB characteristics and the potential variation in the corresponding GW signals motivates a thorough investigation of the possible outcomes of binary compact object (BCO) mergers. BCOs may form through evolution of primordial binaries or through dynamical processes in star clusters (O’Leary et al. 2009; Lee et al. 2010). The latter population motivates this study of BH-NS interactions for systems which are initially marginally unbound.

Star clusters at the centers of galaxies undergo mass segregation, resulting in heavier objects concentrated toward the center (see, e.g. Bahcall & Wolf 1977). Recent Fokker-Plank models suggest that the Galactic nuclear cluster (NC) should have ~ 1800 BHs and ~ 400 NSs in the central 0.1 pc (Hopman & Alexander 2006). Such clusters are thus promising sites for BH-NS close encounters. Using models of galactic NCs, O’Leary et al. (2009) calculate the rate of binary BH formation through GW emission in close encounters. They find corresponding Advanced LIGO detection rates between 5 and 2700 per year, and estimate that the BH-NS rate could be around 1% of this. These capture binaries form with relatively small periapsis separations, r_p ; in particular, $\sim 30\%$ form with $r_p \lesssim 10M$, where M is the total mass of the system (Fig. 4 of O’Leary et al. (2009)). (Unless otherwise stated we employ geometric units with $G = c = 1$.) This is due in part to the large velocity dispersion in the cluster core ($\sim 1000 \text{ km s}^{-1}$), but also to gravitational focusing, which may be understood as follows. The total rate is proportional to the cross-section: $\Gamma \propto \pi b^2$, where b is the impact parameter. However, for Newto-

nian hyperbolic orbits with relative velocity w at infinity, $r_p = b^2 w^2 / 2M + O(w^4)$. Thus, the rate is *linearly* proportional to r_p .

Globular clusters (GCs) that have undergone core collapse may also host BCO close encounters due to the high density of compact objects in their cores (Fabian et al. 1975; Grindlay et al. 2006). For example, models of M15 calibrated to the observational velocity dispersion yield a NS fraction of $\sim 55\%$ in the inner 0.2 pc (Dull et al. 1997). Lee et al. (2010) calculate the expected rate of BCO interactions inside M15 as a function of time and then scale these results for GCs with a distribution of half-mass relaxation times. Depending upon the GC evolution model, they find that the global rate for BH-NS collisions (i.e., events for which $r_p \leq R_{\text{NS}} + R_{\text{BH}}$) peaks at $\sim 8 - 25 \text{ yr}^{-1} \text{ Gpc}^{-3}$ at redshifts between $z = 0.36$ and $z = 0.97$, and slowly declines to between 50–85% of peak by $z = 0$. (We obtained the BH-NS collision rate by re-scaling their NS-NS results according to the factors in Table 3 of Lee et al. 2010). For the fiducial BH-NS system considered by Lee et al. (2010), collisions occur at $r_p \leq 2.7M$. Since the rate scales linearly with r_p , this implies an interaction rate $\sim 30 - 100 \text{ yr}^{-1} \text{ Gpc}^{-3}$ with (for example) $r_p \leq 10M$.

Population synthesis models (Belczynski et al. 2010) find comparable rates for *primordial* BH-NS mergers: from $\sim 0.1 \text{ yr}^{-1} \text{ Gpc}^{-3}$ (pessimistic) to $\sim 120 \text{ yr}^{-1} \text{ Gpc}^{-3}$ (optimistic). However, primordial BH-NS binaries will enter the LIGO band with essentially zero eccentricity (Kowalska et al. 2011). Thus, GW signals from BH-NS close encounters should be readily distinguishable due to their significant eccentricities. We further note that the sGRB rate, $8\text{-}30 \text{ yr}^{-1} \text{ Gpc}^{-3}$ (Guetta & Piran 2006), is comparable to the primordial BH-NS rate, and somewhat less than the expected NS-NS merger rate ($30\text{-}400 \text{ yr}^{-1} \text{ Gpc}^{-3}$ (Belczynski et al. 2010)). The estimates of Lee et al. (2010) thus suggest

that close encounters in clusters could contribute significantly to the sGRB progenitor population, especially if their emission is less tightly beamed than that of primordial mergers (Grindlay et al. 2006).

BH-NS mergers in clusters with $r_p \lesssim 10M$ will exhibit complicated behaviors probing the strong field regime of general relativity (GR). For stellar mass BH companions, one cannot treat the NS as a perturbation of the BH spacetime. Furthermore, the non-linear nature of GR will most strongly manifest during a close encounter of the BH-NS. Numerical simulations within full GR are thus the preferred tool for exploring these systems. To date, such simulations have been performed by several groups (Etienne et al. 2009; Kyutoku et al. 2010; Duez et al. 2008; Chawla et al. 2010; Pannarale et al. 2011) (see Duez 2010 for a review). These studies employ quasi-circular initial data, appropriate for primordial systems, and have explored a range of behaviors depending on the mass ratio, the BH spin, the NS equation of state (EOS), and the magnetic field. Our results complement these works by offering a first study within full GR of initially hyperbolic encounters, of relevance to BH-NS capture events and related systems that merge with large eccentricity.

In the remainder of the letter we outline our numerical method, present results of our parameter space survey, and discuss some of their implications. The main result is the striking dependence of the outcome—disk mass, unbound material, and GW signal—on the impact parameter. Though the most “extreme” outcomes might require fine-tuning and hence be rare, there is strong variation over the entire range $r_p \lesssim 10M$ we considered: for a hyperbolic encounter in a NC, this corresponds to roughly 30% of encounters that lead to a bound system. We were not able to follow the larger r_p cases through merger due to lack of computational resources, though certainly a fraction of these should also exhibit similar variability at the time of merger. This suggests that these systems could be a wellspring of varied and interesting GW and electromagnetic emission.

2. NUMERICAL APPROACH

Our 3D numerical code solves the Einstein field equations using finite difference (FD) techniques with Berger and Olinger style adaptive mesh refinement (AMR, Berger & Olinger 1984). The numerical scheme for evolving the spacetime metric is substantively the same as the generalized harmonic method described by Pretorius (2005b,a), except that the FD scheme is fourth order accurate and uses fourth order Runge-Kutta time integration. We model the NS material as a perfect fluid and solve the hydrodynamic energy-momentum and continuity equations using conservative high-resolution shock-capturing schemes with second order Runge-Kutta time integration, and enforce strict conservation at AMR boundaries using the flux correction method of Berger & Colella (1989). We have implemented several methods for calculating inter-cell fluxes (HLL, Harten et al. 1983; the Roe solver, Eulderink & Mellema 1995; and the Marquina flux, Marquina et al. 1992) and for reconstructing fluid primitive variables at cell interfaces (MC and minmod, Toro 1997; PPM, Colella & Woodward 1984; and WENO-5, Tchekhovskoy et al. 2007). Unless otherwise noted, the

simulations described below were performed with HLL and WENO-5. Our hydrodynamics scheme allows for any EOS of the form $P = P(\rho, \epsilon)$ (e.g., Γ -law, piecewise polytrope, and tabular EOSs). We have tested the new hydrodynamics sector of our code on problems including 1D and 2D Riemann problems, Bondi accretion, and single NSs. More details on our code and tests will be presented in Stephens et al. (2011).

For this first study the only parameter we vary is the initial periapsis separation. The BH and NS have a 4:1 mass ratio, and both are initially non-rotating. The NS is modeled as a TOV star with a broken Γ -law EOS (labeled “HB” in Read et al. 2009 and including a thermal component to allow for shock heating) and has mass $1.35M_\odot$ and radius 11.6 km. The initial orbital parameters describe a hyperbolic encounter with relative velocity $w = 1000 \text{ km s}^{-1}$, corresponding to the central region of a NC (O’Leary et al. 2009). These orbits are nearly parabolic, with $e - 1 \sim O(10^{-5})$, and hence the close-encounter behavior also adequately describes such events in GCs. We superimpose initial data for the BH and NS at an initial separation of $50M$ (498 km) with initial velocities according to a Newtonian orbit with the desired r_p . Though these superposed initial data do not strictly satisfy the constraint equations except at infinite separation, tests performed at various initial separations indicate that $50M$ is sufficiently large that the constraint violation does not appreciably affect the system (relative to truncation error).

3. RESULTS AND DISCUSSION

We consider a range of periapsis separations from $r_p/M = 5.0$ to 15 (*i.e.*, 50 to 150 km). (Henceforth, we will consider r_p to be normalized by M .) In all of these cases, sufficient energy is carried away by GWs to result in a bound system. Our simulations exhibit three types of behavior: (1) a direct plunge ($r_p = 5.0, 5.83, 6.67, 6.81$), (2) following the initial periapsis passage, a single elliptical orbit and then a plunge ($r_p = 6.95, 7.22, 7.5$), and (3) following the initial periapsis passage, a long-period elliptical orbit ($r_p = 8.75, 10.0, 12.5, 15.0$). For the latter group (and the high resolution $r_p = 7.5$ run), the entire orbit is prohibitively long to simulate, and we focus on the burst of GWs associated with the first periapsis passage. For one case in each class ($r_p = 5.0, 7.5, 10.0$) we ran three simulations with different characteristic mesh spacings (but always with 7 refinement levels) for convergence studies. At $t = 0$, the low (medium, high) resolution run had finest meshes covering the BH and NS of roughly 80^3 ($100^3, 150^3$) cells, resolving the NS diameter with ~ 40 (50, 75) cells and the BH horizon diameter with ~ 70 (85, 130) cells. (We note that the level structure is set by truncation error estimates and is adjusted with time.)

All other simulations were run at medium resolution. Unless otherwise noted, results will be reported for medium resolution, with error bars (where appropriate) computed from convergence calculations. Our simulations employ compactified coordinates such that the outer boundaries extend to spatial infinity. Thus, the global (ADM) M and J should be conserved. In practice, however, we must evaluate these quantities at a finite distance, making them subject to gauge artifacts, some propagating outward from the central BH/NS re-

gion from $t = 0$. For $t < 200M$, an extraction sphere of $300M$ is free of propagating artifacts, whence M (J) is conserved to better than 0.3 (2.0)% for all cases at medium resolution.

Based on the above of runs, some guidance from perturbative results (Peters & Mathews 1963; Turner 1977; Berry & Gair 2010), and a zoom-whirl geodesic analogue of the two body problem (Pretorius & Khurana 2007), we conjecture the following qualitative behavior as a function of r_p for initial encounters resulting in a bound system.

Consider n , the non-negative, integer number of periapsis passages before disruption/plunge, and r_p^i , the periapsis distance on the i^{th} encounter for $1 \leq i \leq n$. Define r_p^{n+1} to be an *effective* periapsis distance for the final close encounter (i.e., the corresponding r_p before the disruption/plunge part of the final encounter). Group (1) above has $n = 0$, group (2) $n = 1$, and group (3) $n \geq 1$. The behavior of a close encounter will depend sensitively on the distance $\delta r_p^i = r_p^i - r_c$ between r_p^i and a radius r_c of an effective *unstable circular* orbit with the *same* energy and angular momentum. If δr_p^i is sufficiently small (relative to M), the orbit will exhibit a whirl phase, where it asymptotes to a nearly circular orbit. The smaller δr_p^i , the longer the duration of the whirl, with a maximum when $\delta r_p^i = 0$ that equals the time required for the binary to lose its *excess* orbital kinetic energy, either via GW emission or tidal transfer of energy to the NS material. The excess energy is the difference between the total energy of the binary entering the whirl phase and a putative binary on a *quasi-circular* inspiral at r_c .

Because of the requirement that δr_p^i be small, we only expect the possibility of significant whirling near the ultimate or penultimate encounter. If δr_p^i is negative, the whirl will directly transition to a plunge. If positive and small, there will be a separation following the whirl; however the effective r_c for the next encounter *increases* while r_p^i *decreases* due to GW emission, and since this is quite sizeable for our 4:1 mass ratio system, δr_p^{i+1} will likely be negative, resulting in a subsequent plunge. Furthermore, the separation where the NS starts to be tidally disrupted is within the radii of unstable whirl orbits, hence the NS will not survive any prolonged whirl phase. Prior encounters (for larger n cases) will not exhibit significant whirling, and while δr_p^i is large the orbital evolution could better be described as a series of precessing ellipses with decreasing eccentricity and semi-major axis.

Considering the number of orbits n as a function of the *initial* r_p , $n(r_p)$ is monotonically increasing, and the values of r_p where one could see a notable final whirl would be near the steps in $n(r_p)$. The most pronounced whirl behavior will occur for small $n(r_p)$; as $n(r_p)$ increases, the amount of excess kinetic energy left over once the final orbit is reached decreases, and for sufficiently large n the late stages will essentially follow a quasi-circular inspiral.

Figure 1 illustrates some of the varied phenomena encountered near the transition between $n(r_p) = 0$ and $n(r_p) = 1$, occurring at $r_p \approx 6.88 \pm 0.08$. Most striking is the amount of rest mass remaining after the merger as a function of r_p (Table 1). For cases in which the NS plunges without significant disruption, such as $r_p = 5$ or

$r_p = 7.5$, less than 1% of the initial mass is available to form an accretion disk. However, for r_p closer to the first transition ($r_p = 6.67$ and 6.81 , see Figure 1), the NS is stretched into a long tidal tail, and a sizeable amount of bound material is left to form an accretion disk—12% of the initial NS rest mass for $r_p = 6.81$.

Figure 2 shows the approximate rate of fallback as a function of time for $r_p = 6.81, 6.95, 7.22$, and 7.5 . This is the rate at which material on elliptical orbits is expected to return to the accretion disk (see Rosswog 2007). (These accretion rates are likely upper limits since they do not account for nuclear burning, see Metzger et al. 2010.) The fallback rate is larger for cases with larger disk masses, such as $r_p = 6.81$, but all cases exhibit an approximate $t^{-5/3}$ falloff. This time dependence was predicted for stellar disruptions around supermassive BHs by Rees (1988). It appears unlikely that BH-NS mergers with fallback rates as in Fig. 2 will be able to explain sGRBs with extended emission (see, e.g., Norris & Bonnell 2006) if this emission is due to feeding of the accretion disk at late times. For example, by $t \approx 100$ s, the luminosity for the $r_p = 6.81$ case would be only $L \sim \eta \dot{M} c^2 \sim 2 \times 10^{42}$ erg/s (assuming an efficiency $\eta = 0.1$).

Table 1 also shows the total energy and angular momentum lost to GWs for r_p between 5 and 12.5. For the cases that we followed through merger, we find 0.7-1.7% of the total mass lost to GW energy, and estimate the final spins of the BHs to be $(0.49 \pm 0.01, 0.45, 0.37, 0.47, 0.50, 0.50)$ for $r_p = (5.00, 6.67, 6.81, 6.95, 7.22, 7.50)$ respectively. The energy loss is largest for the transitional case ($r_p = 6.95$), which has a large pulse from the whirling first passage and a second burst from the merger (Fig. 3). Table 1 also shows the GW losses for the initial encounter in cases where the NS survives the periapsis passage (columns 5 and 6). These fly-by pulses can be compared with the prediction of Turner (1977) (Fig. 3, lower panels, and Fig. 4), who used the Newtonian orbit together with quadrupole physics for the GW emission, which we will call the *Newtonian Quadrupole Approximation* (NQA). Our waveforms show roughly the same pulse shape as the NQA prediction but have larger amplitudes for the smaller r_p cases. At $r_p = 15$ we find the gravitational waveform from the initial fly-by to be indistinguishable from the NQA prediction at our resolution ($\pm 10\%$).

The enhancement in GW energy losses for close encounters may be due (in part) to zoom-whirl-like behavior. Figure 4 shows the GW energy loss as a function of r_p , along with the NQA prediction and a fit consistent with zoom-whirl dynamics (Pretorius & Khurana 2007) in the regime ($r_p \lesssim 10$) where we start to see significant departures from the NQA approximation.

4. CONCLUSIONS

An interesting result of this general relativistic study that is qualitatively consistent with previous Newtonian studies (e.g. Lee et al. 2010), is the great variability of the outcome as a function of impact parameter. For example, the remnant disk masses following merger range from nearly zero up to $\sim 0.3M_\odot$. Mergers leading to significant disks occur in a small (but not negligible) region of parameter space and could produce a sGRB.

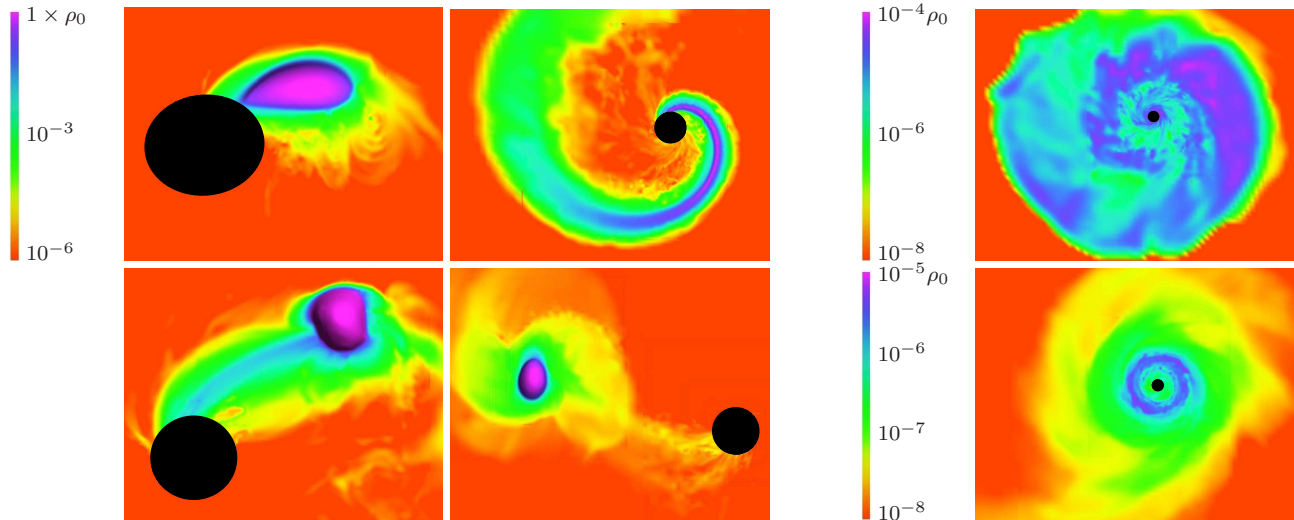


FIG. 1.— Rest mass density in the equatorial plane from BH-NS simulations with varying r_p . The four panels on the left show (left to right, top to bottom, same color scale): (1) the BH and NS merging ($t = 6.82$ ms, $r_p = 5$), (2) the NS being stretched into a long tidal tail ($t = 9.97$ ms, $r_p = 6.81$), (3) a brief mass transfer episode during the NS’s first periapsis passage ($t = 8.78$ ms, $r_p = 6.95$), and (4) the NS’s subsequent distortion ($t = 10.6$ ms, $r_p = 6.95$). On the right is a nascent accretion disk (top, $t = 12.3$ ms, $r_p = 6.67$), and a late-stage accretion disk (bottom, $t = 38.2$ ms, $r_p = 7.5$, low resolution, PPM). The color scale is logarithmic with units of the initial maximum density ($\rho_0 = 8.3 \times 10^{14}$ g cm $^{-3}$). The black hole is roughly the same coordinate size in all panels ($R_{\text{BH}} = 16$ km), which can be used to infer the relative scale of each snapshot.

r_p	$M_0/M_0(t=0)^a$	$M_{0,u}/M_0(t=0)^b$	τ_{acc} (ms) ^c	First periapsis ^d		Total ^e	
				$\frac{E_{\text{GW}}}{M} \cdot 10^2$	$\frac{J_{\text{GW}}}{M^2} \cdot 10^2$	$\frac{E_{\text{GW}}}{M} \cdot 10^2$	$\frac{J_{\text{GW}}}{M^2} \cdot 10^2$
5.00	0.005	0.0	25	0.67(0.87)	4.14(4.86)
6.67	0.107	0.056	130	1.29	9.10
6.81	0.221	0.101	40	1.19	9.60
6.95	0.018	0.003	47	0.697	7.33	1.65	13.9
7.22	0.013	0.001	16	0.358	4.48	1.18	10.2
7.50	0.009	0.003	7.6	0.242(0.147) ^f	3.44(2.46)	1.03	44.7
8.75	0.073	1.58
10.0	0.033(0.027)	0.97(0.88)
12.5	0.011	0.46

TABLE 1
DISK PROPERTIES AND GW ENERGY AND ANGULAR MOMENTUM LOSSES

^aRest mass remaining outside the BH shortly after merger, normalized by the initial total rest mass.

^bUnbound rest mass estimated using local fluid velocities.

^cRough *initial* accretion timescale ($\tau_{\text{acc}} = M_0/\dot{M}_0$) evaluated shortly after merger.

^dEnergy and angular momentum lost to GWs during the first close encounter.

^eTotal GW energy and angular momentum losses for cases which were followed through merger.

^fResults are from medium resolution runs; values in parentheses are Richardson extrapolated estimates using low and high resolutions, where available. Note that the relatively large error for $r_p = 7.5$ (and to a lesser extent $r_p = 5, 10$) is due in part to truncation error altering the actual periapsis by a small amount, and in this regime the GW emission is highly sensitive to binary separation (Figure 4).

In follow up work we plan to extend the parameter space survey, varying the NS EOS and BH spin. We also intend to explore the detectability of these events with GW detectors, and conclude with brief preliminary comments. These signals may be difficult to detect with instruments such as LIGO since they lack a long inspiral phase and most of the power is at high frequencies (1500-2000 Hz for the masses considered here). Using the broadband AdLIGO noise curve, we find sky-averaged SNR of 3-9 for $r_p = 5 - 10$, assuming a distance of 100 Mpc. Scaling the GW emission up to $(M_{\text{NS}}, M_{\text{BH}}) = (2, 8)M_{\odot}$ and assuming optimal orientation gives SNR of 8 out to 340 Mpc for $r_p = 7.5$. En-

counters with larger r_p could be easier to detect since they will have a number of fly-by GW bursts before the merger. Given that some BH-NS capture binaries emit the majority of their GW power at the high frequency end of the LIGO noise curve and could be relatively weak (both in terms of GW emission and extrapolated electromagnetic emission based on disk mass), it may be a worthwhile exercise to revisit the analysis of GRB 070201 (Abbott et al. 2008) with burst-templates adapted to capture driven BH-NS encounters.

We thank Adam Burrows, John Friedmann, Roman Gold, Benjamin Lackey, and Richard O’Shaughnessy

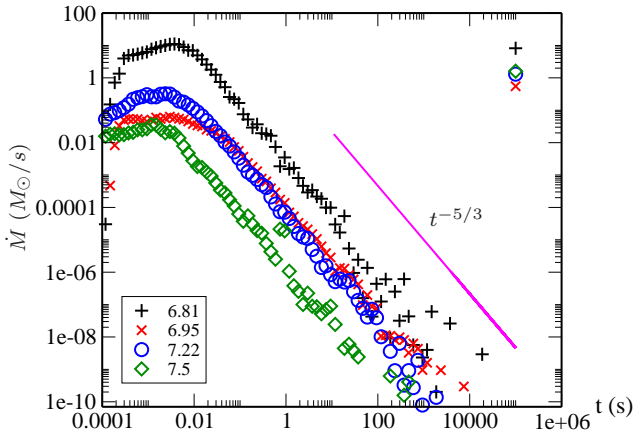


FIG. 2.— Approximate fallback accretion rates for $r_p = 6.81$, 6.95, 7.22, and 7.5. These rates are evaluated at times ranging from 1.0 to 2.2 ms after the approximate time when the BH accretion rate plateaus following the merger. For this diagnostic, we consider the fluid in each cell as a ballistic particle and take its orbital period as the approximate fallback timescale. The instantaneous BH accretion rates evaluated at the same time are shown at the upper right (arbitrary abscissa).

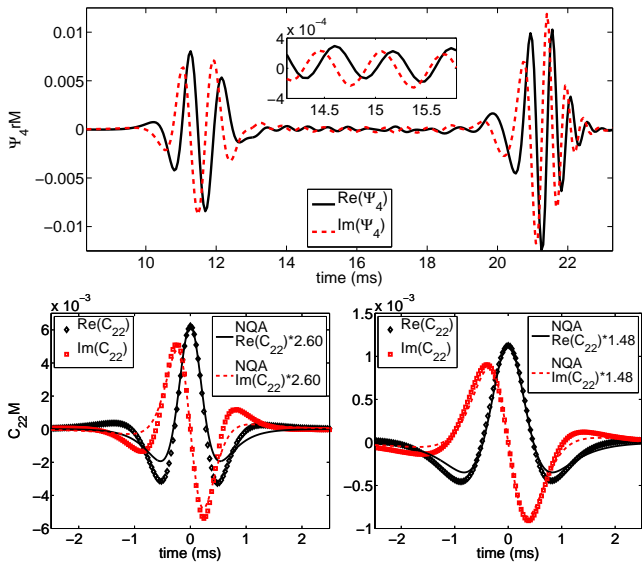


FIG. 3.— (*upper panel*) The Newman-Penrose scalar Ψ_4 on the z -axis (orthogonal to the orbit) for $r_p = 6.95$. The first pulse is from the initial close encounter, the second from the merger-ringdown. Between the pulses there is an oscillation due to the rotating, distorted neutron star, which is significantly torqued during the first encounter. Here $t = 0$ corresponds to the start of the simulation. (*lower panels*) The real and imaginary components (black diamonds and red squares) of the $l = 2$, $m = 2$ spherical harmonic of $r\Psi_4$ for $r_p = 7.5$ (left) and $r_p = 10$ (right). For comparison the NQA analytical results are shown multiplied by an overall factor so that the magnitude and phase match at peak ($t = 0$).

for useful conversations. This research was supported by the NSF through TeraGrid resources provided by NICS under grant TG-PHY100053, the Bradley Program fellowship (BCS), the NSF Graduate Research Fellowship under grant DGE-0646086 (WE), NSF grants PHY-0745779 (FP) and PHY-1001515 (BCS), and the Alfred P. Sloan Foundation (FP). Simulations were also run on the **Woodhen** cluster at Princeton University.

REFERENCES

- Abbott, B., et al. 2008, *Astrophys. J.*, 681, 1419
 Abramovici, A., et al. 1992, *Science*, 256, 325
 Bahcall, J. N., & Wolf, R. A. 1977, *ApJ*, 216, 883
 Belczynski, K., Dominik, M., Bulik, T., et al. 2010, *ApJ*, 715, L138
 Berger, M., & Colella, P. 1989, *J. Comp. Phys.*, 82, 64
 Berger, M. J., & Oliger, J. 1984, *J. Comp. Phys.*, 53, 484
 Berry, C.P.L., & Gair, J. 2010, *Phys. Rev. D*, 82, 107501
 Chawla, S., Anderson, M., Besselman, M., et al. 2010, *Phys. Rev. Lett.*, 105, 111101
 Colella, P., & Woodward, P. R. 1984, *J. Comp. Phys.*, 54, 174
 Duez, M. D. 2010, *Class. and Quant. Grav.*, 27, 114002
 Duez, M. D., Foucart, F., Kidder, L. E., et al. 2008, *Phys. Rev. D*, 78, 104015
 Dull, J. D., Cohn, H. N., Luggner, P. M., et al. 1997, *ApJ*, 481, 267

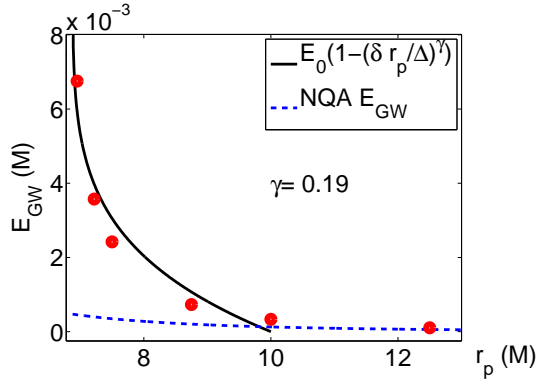


FIG. 4.— Energy lost to GWs during the initial close encounter (i.e. excluding merger) as a function of r_p . The functional form $E_0(1 - (\delta r_p/\Delta)^\gamma)$ (solid line), motivated by zoom-whirl dynamics, is a fit to the simulation results (red dots). $\delta r_p = \delta r_p^1 = r_p^1 - r_c$ as discussed in the text; here $r_p^1 = r_p$. E_0 is the difference in energy between a quasi-circular orbit and an $e \approx 1$ orbit both with $r_p = r_c$. Δ is the range over which zoom-whirl like behavior dominates the GW emission energetics. γ is a parameter that in the geodesic analogue is related to the instability exponent of the corresponding unstable circular orbit; here, we use it as our fitting parameter. The NQA approximation is the dotted line.

Etienne, Z. B., Liu, Y. T., Shapiro, S. L., & Baumgarte, T. W. 2009, *Phys. Rev. D*, 79, 044024
 Eulderink, F., & Mellema, G. 1995, *A&AS*, 110, 587
 Fabian, A. C., Pringle, J. E., & Rees, M. J. 1975, *MNRAS*, 172, 15
 Grindlay, J., Portegies Zwart, S., & McMillan, S. 2006, *Nature Physics*, 2, 116

Guetta, D., & Piran, T. 2006, *A&A*, 453, 823
 Harten, A., Lax, P., & van Leer, B. 1983, *SIAM Rev.*, 25, 35
 Hopman, C., & Alexander, T. 2006, *ApJ*, 645, L133
 Kowalska, I., Bulik, T., Belczynski, K., Dominik, M., & Gondek-Rosinska, D. 2011, *A&A*, 527, A70
 Kyutoku, K., Shibata, M., & Taniguchi, K. 2010, *Phys. Rev. D*, 82, 044049
 Lee, W. H., Ramirez-Ruiz, E., & van de Ven, G. 2010, *ApJ*, 720, 953
 Marquina, A., Marti, J. M., Ibanez, J. M., Miralles, J. A., & Donat, R. 1992, *A&A*, 258, 566
 Metzger, B. D., Arcones, A., Quataert, E., & Martínez-Pinedo, G. 2010, *MNRAS*, 402, 2771
 Narayan, R., Paczynski, B., & Piran, T. 1992, *ApJ*, 395, L83
 Norris, J. P., & Bonnell, J. T. 2006, *ApJ*, 643, 266
 O’Leary, R. M., Kocsis, B., & Loeb, A. 2009, *MNRAS*, 395, 2127
 Pannarale, F., Tonita, A., & Rezzolla, L. 2011, *ApJ*, 727, 95
 Peters, P., & Mathews, J. 1963, *Phys. Rev.*, 131, 435
 Pretorius, F. 2005a, *Phys. Rev. Lett.*, 95, 121101
 —. 2005b, *Class. and Quant. Grav.*, 22, 425
 Pretorius, F., & Khurana, D. 2007, *Class. and Quant. Grav.*, 24, S83
 Read, J. S., Markakis, C., Shibata, M., et al. 2009, *Phys. Rev. D*, 79, 124033
 Rees, M. J. 1988, *Nature*, 333, 523
 Rosswog, S. 2007, *MNRAS*, 376, L48
 Stephens, B. C., East, W. E., & Pretorius, F. 2011, in prep.
 Tchekhovskoy, A., McKinney, J. C., & Narayan, R. 2007, *MNRAS*, 379, 469
 Toro, E. 1997, *Riemann Solvers and Numerical Methods for Fluid Dynamics* (Berlin, Germany: Springer)
 Turner, M. 1977, *ApJ*, 216, 610